(Received 11 October 2025, Accepted 11 December 2025, Scheduled 6 January 2026)

Au Nanopatterned LT-GaAs Based H-Shaped Photoconductive Antenna for Terahertz Applications

Sheo K. Mishra[1], Palakkal Mohamed Mashood[2], Ashish Singh[3,*], Shekhara Kavitha[4,*], Himanshu Singh[5,6], and Ravi S. Saxena[7,*]

[1]*Nanoscale Engineering and Sustainable Technology (NEST) Laboratory Department of Physics, Indira Gandhi National Tribal University, Amarkantak M. P., India*
[2]*Department of Physics, IGNTU Amarkantak, M. P., India*
[3]*Department of Computer and Communication, NMAM Institute of Technology (NMAMIT) Nitte Nitte (Deemed to be University), Udupi, India*
[4]*Department of Electronics and Communication, NMAM Institute of Technology (NMAMIT) Nitte Nitte (Deemed to be University), Udupi, India*
[5]*Department of Metallurgical and Materials Engineering, Indian Institute of Technology Kharagpur, India*
[6]*Department of Mechanical Engineering, School of Engineering Sciences, Ramdeobaba University, Nagpur 440013, India*
[7]*Department of Electronics & Communication GMRIT, India*

ABSTRACT: This manuscript presents the design of a nanopatterned H-shaped photoconductive antenna on an LT-GaAs substrate for terahertz applications. The use of gold nanoparticles and Si lens in the gap between two electrodes improves the photoconductive conductive antenna's low efficiency. It is noticed that the proposed PCA resonates at 1.35 THz with −24.2 dB, 1.65 THz with −22.1 dB, and 2.4 THz with −21.32 dB reflection coefficient. Further, with the Si lens, PCA resonates at 2.15 THz with a −30.2 dB reflection coefficient. Moreover, the nanopatterned H-shaped photoconductive antenna resonates at 1.7 THz with the minimum reflection level of −40 dB. These results indicate that the reflection in the photoconductive antenna can be reduced using the nanopatterning technique. This further increases the efficiency of the photoconductive antenna. The proposed H-shaped photoconductive antenna is designed and optimised using the COMSOL Multiphysics platform.

1. INTRODUCTION

Photo-Conductive Antennas (PCAs) and their various derivatives play a crucial role in different fields because the device works at terahertz frequency region such as Artificial Intelligence (AI) and 6G wireless communication [1, 2], imaging and sensing [3], transferring vast amounts of information very swiftly and fast [4, 5], detection of dangerous objects that threaten national security [6], revealing hidden weapons [7, 8], process control [9], and in the medical field [10, 11]. Operating in the low-terahertz frequency region broadens the possibilities of how terahertz gets enhanced with a wide variety of applications. Working on a photoconductive antenna with a dipole structure gives miniaturization of the device with sensitivity and high efficiency. The dipole structure enables light that is applied to focus on a particular region [12]. This increases the Surface Plasmon Polaritons (SPP) around that region. This will enhance terahertz wave emission from a photoconductive antenna [13–15]. A photoconductive antenna is simulated to increase its power efficiency. To accomplish this, the COMSOL Multiphysics application is employed to implement the Maxwell wave equation describing optical interaction [16–20].

The photoconductive antenna was introduced by Auston and his group. They invented two metal electrodes on the base of a photoconductive substrate. An Auston switch with a photoconductive antenna contains two lasers with different wavelengths to turn the switch on and off [21]. After their invention, a lot of variants were produced, such as variants in the structure of the electrode and the gap between them [15]. This paved the way to produce PCA with higher efficiency. Further studies with the decoration of nanostructures or nanoparticles in the gap of PCA showed increased conversion of optical to THz radiation efficiency.

The research work on nanopatterned PCA started with Park et al. [22], and they demonstrated the first augmentation of PCA for THz radiation using plasmonic nanostructure arrays. The commonly used bow-tie antenna was printed on an SI-GaAs substrate with periodic nanostructures created using electron beam lithography. Park's article compared four different types of nanostructures: two square arrays and two grating arrays with widths of 75 and 150 nm, respectively. Measurements revealed that 75 nm square arrays show the lowest reflectance under 800 nm laser light, whereas 75 nm nanorods show the best enhancement performance. The argument presented was that nanorod arrays focus photons over a wider area than nanosquare antennas. As a result, the nanorod shape produces a higher average light concentration on the substrate

* Corresponding authors: Shekhara Kavitha (hereiskavitha@gmail.com); Ashish Singh (ashsin09@rediffmail.com); Ravi Shankar Saxena (ravishankar.s@gmrit.edu.in).

TABLE 1. Antenna parameters used in the analysis.

Description	Symbol	Value
Width of Substrate	W	250 µm
Depth of Substrate	D	250 µm
Height of Substrate	H	12.5 µm
Thickness of metal electrode	TM	300 nm
Width of Antenna	WA	230 µm
Antenna Gap	G	5 µm
Thickness of Transmission Line	TL	10 µm
Thickness of Dipole Section	TD	17.5 µm
Width of Dipole	WD	20 µm
Wavelength of incident light	lamr	800 nm
PML Thickness	PML	20 µm
Incident Power	Pin	10 mW

than the nanosquare structure. This structure outperformed standard PCA in the 0.1–1.1 THz range by a factor of 2.27. According to Lai et al. [23], manganese ferrite nanoparticles ($MnFe_2O_4$ NPs) have been shown to improve semiconductor surface photoconductivity significantly. They conducted experimentally using THz Time-Domain Spectroscopy (THz-TDS), the optical characterization of photo-excited carriers of silicon covered with $MnFe_2O_4$ NPs [23]. The experimental data were evaluated using a surface band structure model of semiconductors. Furthermore, photoconductive antennas coated with $MnFe_2O_4$ NPs increased THz radiation output effectiveness and signal-to-noise ratio [23]. This study shows the dependency of the shape of nanoparticle on the response of PCA. Bashirpour et al. [24] presented an outstanding solution that involves a zinc oxide Nanorod Array (ZnO NR) acting like an optical antenna over a silicon nitride layer in the gap, and this arrangement increases the photocurrent. Hence, terahertz signal is also enhanced. The silicon nitride layer acts as an antireflection layer in the PCA. The nanorods are created in the gap through hydro thermal technique. This method is easy, inexpensive, and compatible in comparison to other methods used for nanoantenna design. This new structure enhances the power almost four times higher than the other antireflective layered PCA designs for 0.1–1.2 THz [24]. This study uses the shape of nanoparticles is a factor of dependence while studying the response. Murakami et al. [25] used sputtering of Au nano islands to create an LT-GaAs-based plasmonic photoconductive antenna, and evaluated its THz detection characteristics. As a consequence, they successfully increased the sensitivity by 29% and 40% at 800 nm and 1560 nm, respectively. Surdi et al. [13] aimed to increase the emission efficiency of a terahertz PCA by nanopatterning it using Gold Germanium (AuGe) nanopatterns. Nano-patterns having geometrical characteristics tailored for a certain optical frequency tend to induce localized surface plasmon resonance, resulting in localized electric field-amplifying factors. This localized field augmentation increases the number of produced photocarriers, which multiplies the THz emission output by a factor of 4 [13]. They also simulated surface plasmon polaritons of AuGe on the surface of the GaAs substrate and

TABLE 2. Input parameters used in the analysis.

Incident Power	10 mW
Electric Field	1 V/m
Propagation Constant	Ewfd.k0

compared them. In [26] by Arora et al., a computational methodology was used to construct effective terahertz photoconductive antennas. Recently, some of the researchers designed photoconductive antennas for terahertz application such as De Vetter et al. [27] demonstrated a large area digitated photoconductive antenna using highly resistive metal to make the field uniform for the terahertz applications. Deumer et al. [28] designed a photoconductive antenna integrated with optical waveguides to increase the sensitivity of terahertz detection. Chen et al. [29] designed a novel terahertz noise source using a photoconductive antenna. The literature shows that there is scope for further improvement in the efficiency of the PCA in this regard, two designs are developed, optimized, and tested using the RF and wave optics modules in COMSOL Multiphysics, a commercial finite element method solver in this work. For this optimized design, optical response is simulated using femtosecond optical pulse excitation. The semiconductor module is then used to investigate the electrical response of the 2D THz-PCA. The results support the efficient creation of THz-PCA by detecting transient current gathered at the electrode terminals, resolving the THz PCA's low output power problem [26]. The literature shows that the major concern with the photoconductive antenna is its low efficiency. There are several methods, such as the use of nanoantennas, optical waveguides, metal layers, doping and hybrid structures, mentioned in the several research papers to overcome the limitation of photoconductive antennas. In this work, a simple method of nanopatterning and the Si lens technique are used.

In this manuscript, an H-shaped PCA is designed using LT-GaAs substrate for terahertz applications using COMSOL Multiphysics simulation environment. The efficiency of the proposed PCA is improved using the nanopatterning technique. The detailed analysis is performed by varying the gap between the gold nanoparticles in the nanopattern.

2. MATERIALS AND METHODS

Figure 1 depicts the structure of an H-shaped and bow-tie photoconductive antenna, where the width of the substrate is denoted by W, the depth of substrate D, the height of substrate H, the thickness of metal electrode TM, the width of antenna WA, the antenna gap G, the thickness of the transmission line TL, the thickness of the dipole section TD and the width of the dipole WD. Tables 1 and 2 give the simulation parameters considered for the analysis of an H-shaped PCA in the COMSOL Multiphysics simulation environment. The finite element method is used in the COMSOL Multiphysics software for the simulation of the photoconductive dipole antenna. For the simulation of a PCA, the LT-GaAs substrate is used, which has the following material properties: electrical conductivity $=$ 1000 v/m [26], relative permittivity $=$ 12.9 [26], relative

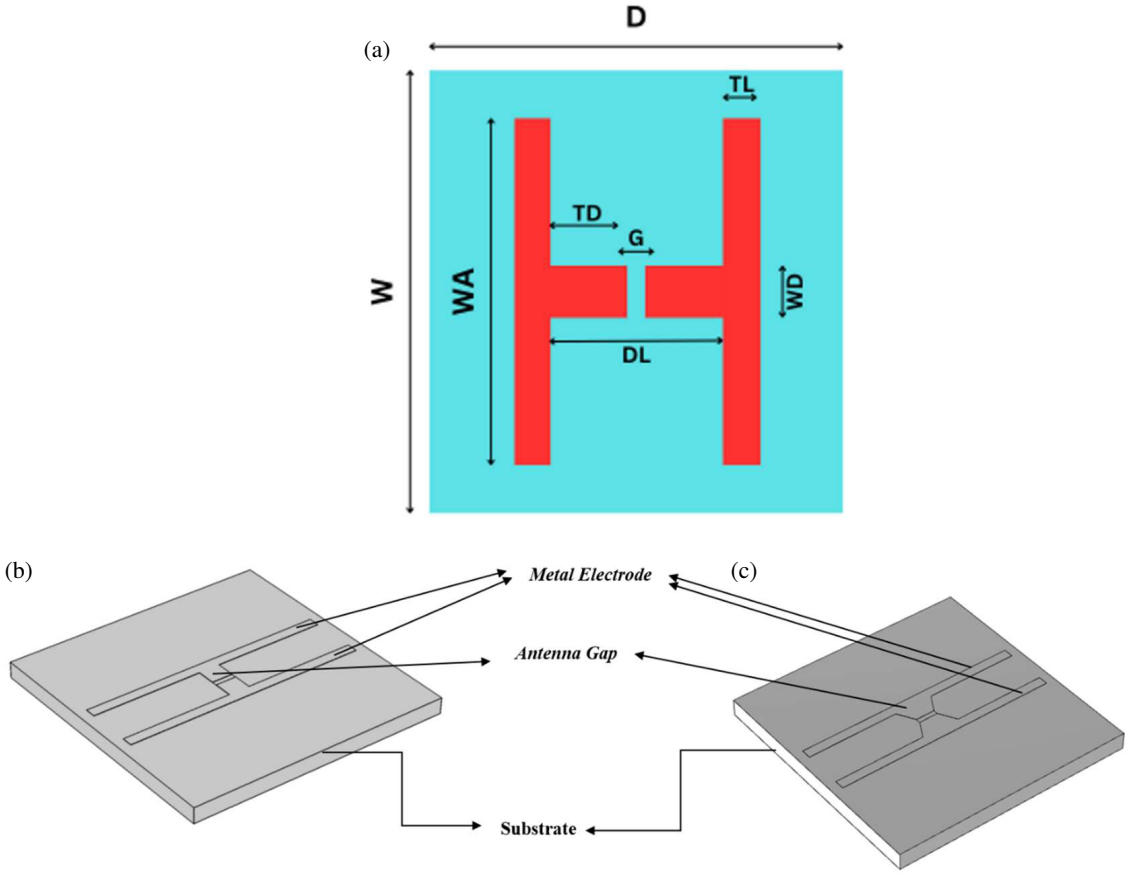

FIGURE 1. Design of photoconductive antenna. (a) Two-dimensional view of H-shaped. (b) Three-dimensional view of H-shaped PCA. (c) Three-dimensional view of Bow-tie.

permeability = 1 [26], refractive index (real) = 3.679 [30], refractive index (imaginary) = 0.085 [30]. For the purpose of electrodes, gold (Au) of a few hundred nanometers thick is used because of its good conductivity and stability. Hence, most current flows in a very small region near the conductor's surface. For the simulation, Au thin films are used as nanopatterns with optical properties. These nanopatterns have a rectangular structure with a width of 500 nm and a thickness of 40 nm. The design is optimized using COMSOL Multiphysics and for the optimized design, optical response is simulated for femtosecond optical pulse excitation. The semiconductor module is then used to investigate the electrical response of the 2D THz-PCA. The results support the efficient creation of THz-PCA by detecting transient current gathered at the electrode terminals, resolving the THz PCA's low output power problem [26].

The length of the dipole is given by Equation (1),

$$DL = 2*TL+G \tag{1}$$

The effective length of the PCA is given by Equation (2),

$$EL = 2*TL+2*TD+G \tag{2}$$

The length and width of the dipole are related by the parameter aspect ratio which is given by Equation (3) [31]

$$\eta = (DL/WD) \tag{3}$$

The dimensions of the proposed photoconductive antenna such as substrate thickness and length are optimized in COMSOL Multiphysics. The proposed antenna is simulated using the Perfectly Matched Layer boundary by adding physics such as far-field domain, electrical connections, Wave-Optics Module, scattering boundary, and identifying the location of illuminating light (Port). The physics-controlled meshing technique governed by frequency domain electromagnetic with coarse element size in COMSOL Multiphysics is selected for the meshing of the proposed geometry. The Wave-Optics Module and Semiconductor Module are coupled using optical transition feature in the COMSOL Multi-Physics. The simulations are performed using the optical pulse of wavelength 800 nm with 10 mW power level to excite the proposed photoconductive antenna. The proposed terahertz antenna can be fabricated using lithography techniques, such as electron beam lithography, and can be analyzed using the microscopic techniques. The nanopatterning of the antenna can be uniformly and precisely placed on a photoconductive using this advanced nanofabrication techniques.

2.1. The Terahertz PCA Materials

The study of terahertz materials required for the design of the photoconductive antenna is the most considered research field. This is due to the fact that there is no natural material that can emit terahertz signals strongly and efficiently [32]. The material's intrinsic carrier lifetime is not long enough to cover such high-frequency bands as THz. Therefore, material stud-

TABLE 3. Characteristics of different PCA substrate material.

Element	Carrier Lifetime (ps)	Mobility ($cm^2\ V^{-1}\ s^{-1}$)	Resistivity (Ω cm)	Breakdown field ($V\ cm^{-1}$)
SI-GaAs	Several Hundred [41]	8500 [42]	$\sim 10^7$ [43]	$4 * 10^5$ [42]
LT-GaAs	< 1 [44]	200 [41]	$> 10^7$ [45]	$5 * 10^5$ [41]
LT-In GaAs	Higher than LT-GaAs [46]	26 [47]	760 [47]	$\sim 6 * 10^4$ [47]

ies for THz are of vital importance for decreasing the carrier lifetime. The study of material properties for optoelectronic devices is still in its infancy [33, 34]. In Auston's first THz antenna, silicon was the photoconductive substrate material [35]. Silicon's bandgap is 1.12 eV at 300 k, with an intrinsic resistance of $2.3 * 10^5\ \Omega$ cm. The indirect bandgap of the silicon suggests that the valence band maximum and the conduction band minimum are not aligned properly [36]. As a result, optical recombination processes become literally slow. On the other hand, since GaAs exhibits a direct bandgap, photons are emitted with no exchange of phonons with the lattice. GaAs's intrinsic resistivity is $10^8\ \Omega$ cm. Additionally, since GaAs belongs to iii–v groups, the material properties can be modified through the addition of defects in the alloy. The constant evolution of THz antennas has been attributed to the change in the features of GaAs [37]. The photoconductive antenna materials include substrate material (photoactive material), electrode material (usually metal), and antenna lens material for enhancing the radiation (Si lens).

2.2. Substrate Material

In most THz photoconductive antennas, the substrates used are semiconductors, such as Si, GaAs, InGaAs, and LT-GaAs because of their desirable properties, such as an ultra-short carrier, high electron mobility, a high intrinsic resistivity, and a high breakdown voltage [38, 39]. The substrate thickness is another factor that differentiates THz antennas from others. This factor is comparable to the radiation wavelength in terahertz antennas, hence guided waves in the substrates are also considered for the analysis.

In theory, Table 3 illustrates the features of the two major THz photoconductive materials (LT-GaAs and SI-GaAs) for optical sources operating at 800 nm. High mobility is a benefit of SI-GaAs. Nevertheless, the input dc bias for SI-GaAs based terahertz antennas is limited due to their smaller breakdown field than LT-GaAs. Furthermore, compared to LT-GaAs, its lower resistivity causes a greater dark current to be generated when there is no laser light, which heats the device and causes it to break down more quickly. SI-GaAs's high carrier lifetime, which restricts the spectral range that may be achieved and increases noise, is another problem. There are many ways to fabricate InGaAs, which, in consequence, causes variations in the behavior of the material. The breakdown field, resistivity, and carrier lifespan of LT-InGaAs are all extremely low at 1550 nm [40]. The main benefit is that it can be used as reliable optical sources, which can significantly make the terahertz system economical compared to other materials. Because of its superior combined properties, LT-GaAs is widely used photoconductive material in terahertz devices.

For the simulation of a proposed design, the LT-GaAs with the following material properties: electrical conductivity $=$ 1000 V/m [26], relative permittivity $=$ 12.9 [26], relative permeability $=$ 1 [26], refractive index (Real) $=$ 3.679 [30], refractive index (Imaginary) $=$ 0.085 [30] are considered.

2.3. Electrode Material

Usually, in a THz photoconductive antenna, the electrodes are made up of metals and metal alloys such as an AuGe and Ti/Au layers. A stacked combination of metals has also been used for more efficient conductors and the patterning of these metals is easy and cost-efficient. Gold has extraordinary chemical stability, reflectivity, and electrical conductivity. Additionally, these properties also depend on the form of the gold such as bulk, thin film, and nanoparticle. Because of its distinct properties and adaptability, gold is used in both conventional and cutting-edge optical technologies. In this design, a few hundred nanometres thick Au electrode is used because of its good conductivity and stability. Hence, mostly current flows in a small region close to the surface of the conductor. In COMSOL, the optical material library gives the data for the gold electrode (Johnson and Cristy 1972: $n, k = 0.188$–1.937 m), where the material properties are frequency-dependent complex values [48].

2.4. Antenna Lens

A photoconductive antenna without lenses strongly diffracts the signals at the surface-to-air interface. This causes less transmission of the terahertz signal in the PCA and reduces the efficiency due to the high refractive index ($n = 3.4$). The boundary angle for the total reflection can be calculated with the Equation (4):

$$\alpha = \arcsin\left(n^{-1}\right) \sim 17.1^\circ \tag{4}$$

Only the terahertz wave is emitted in the solid angle Ω given in Equation (5):

$$\Omega = 4\pi \sin^2\left(\frac{\alpha}{2}\right) = 2\pi(1-\cos\alpha) = 2\pi\left(1-\sqrt{\frac{n^2-1}{n^2}}\right) \tag{5}$$

Only the terahertz waves emitted at a solid angle Ω will reflect from the substrate and escape. This angle is called escape solid angle defined in Equation (5). The escape solid angle for GaAs with $n = 3.679$ is 0.28. This amounts to a mere 4.4% of the intensity projected forward [9]. With the application of the hemispherical Si lens (the Si lens is transparent to THz radiation if its thickness is less than 0.5 mm), the transmittance

can be increased by more than 50 percent of the photoconductive antenna without the Si lens. It is intended to choose a silicon material for the simulation that has optical properties that enable us to get proper results. For this purpose, silicon material with varying refractive index (Green and Keevers 1995: n: 0.25–1.45, k: 0.25–1.00) [49] is selected.

2.5. Nanopatterns

For the simulation, Au thin films are used as nanopatterns with optical properties. These nanopatterns have a rectangular structure with a width of 500 nm and a thickness of 40 nm. These square patterns allow us to analyze homogenous patterns in nature entirely. Therefore, it signifies that the material used for the electrode, cannot be used for this purpose. So, in this case, a gold nanopattern is used with the material property of thin film (Rosenblatt et al. 2020; 44 nm film, n, k 0.30–2.0) [50]. The conventional theory of surface plasmon dispersion is governed by Equation (6) [17]

$$k_{sppd}=k_0\sqrt{\frac{\varepsilon_{ma}\varepsilon_{mb}}{\varepsilon_{ma}+\varepsilon_{mb}}} \tag{6}$$

where k_{sppd} is the momentum of surface plasmon polaritons, and ε_{ma}, ε_{mb} are the dielectric constants of the metal and dielectric medium. This indicates that k_{sppd} is larger than k_0, i.e., there is a requirement of additional motion to excite surface plasmons from the air. The generation of electron-hole pairs in the photoconductive antenna is described by the generation rate under the optical regime given in Equation (7) [36].

$$G_p=\frac{\propto_p I_p}{\bar{h}\omega_p} \tag{7}$$

where $\propto_p$, I_p, $\bar{h}$, and ω_p are the absorption coefficient, intensity, reduced Planks constant, and frequency of the optical signal, respectively. The rate equation of the process is given in terms of density and lifetime of carriers using Equation (8) [36]

$$\frac{dn_p}{dt}=G_p-\frac{n_p}{\tau_p} \tag{8}$$

The process of nanopatterning enhances the electric field through the plasmonic effect, which increases the electron-hole pair generation. The surface plasmons generated by the nanopattern increases the intensity of the optical field and hence increases generation rate G_p.

3. RESULTS AND DISCUSSIONS

The design parameter optimization of the conventional photoconductive dipole antenna by using structural parameters and analysis of the proposed PCA is depicted in this section. It includes the thickness of the substrate, the radius of the Si lens, the thickness of the electrode metal, and the shape optimization of the dipole structure. Different dipole structures are also discussed. The objective of this work is to introduce a new method to increase the efficiency of PCA by introducing nanopatterns, which is also discussed in this section. The modeling process involves examining the impact of various antenna design characteristics on performance. The parametric analysis is used to optimize the design of the proposed PCA. The parameter variation ranges are carefully chosen while considering manufacturing limits to decrease memory needs for numerical models with several design parameters in parametric research. Each parameter's upper and lower limits are designed to encompass the widest range of values while preserving the geometry of the proposed antenna. Only meaningful parameter values are used in our parametric analysis, taking into account manufacturing constraints.

3.1. Effect of LT-GaAs Substrate Thickness

Figure 2(a) depicts the S_{11} parameter of a THz antenna with the variations in substrate thickness. Fig. 2(a) depicts the S_{11} parameter of a THz antenna with the variations in substrate thickness. This thickness is often greater than the wavelength of terahertz signal, hence introducing surface or substrate modes. Therefore, this influence must be considered in the analysis. A study is conducted by changing the substrate's thickness from 10 µm to 20 µm with a period of 2.5 µm. The designed PCA exhibits resonant peaks at 3.2 THz and 1.7 THz with a reflection coefficient of −13.1 dB and −11.07 dB, respectively, with 10 µm substrate thickness. When the thickness is 12.5 µm, the resonance peaks observed are 1.65 THz and 2.2 THz with −31.5 dB and −13.1 dB reflection. The resonant peaks at 1.65 THz and 1.9 THz with a reflection coefficient of −24.3 dB and −19.3 dB, respectively, at 15 µm substrate thickness and at 17.5 µm 1.65 THz with −22.6 dB, 1.8 THz with −15.5 dB, and at 20 µm 1.65 THz with −17.1 dB and 1.75 THz with −15.3 dB are observed. It is observed that as the substrate thickness increases, the resonance frequency of the PCA decreases. The results describe that for the optimum value of thickness, i.e., 12.5 µm with a resonant frequency of 1.65 THz, the bandwidth of the PCA is around 2.2 THz (1.3 to 3.5 THz). Figs. 2(a1) and (a2) give the 2D radiation pattern in both the electric field and magnetic field at 1.65 THz resonant frequency.

3.2. Effect of Au Electrode Thickness

The influence of gold (Au) thickness on the top layer of the proposed THz antenna is parametrically investigated, as illustrated in Fig. 2(b). The thickness of the metal is varied from 200 nm to 400 nm in steps of 50 nm. The analysis depicts that varying the metal thickness from 200 nm to 400 nm results in a minimal difference in impedance matching across the band. The results depict that as the thickness of the metal electrode increases, even though there is no change in the resonance frequency of the antenna, the reflection in the PCA drastically changes. The observed reflection coefficients at 1.65 THz are −26.7 dB, −31 dB, −31.75 dB, −31.59 dB, and −25.7 dB, respectively, at the thicknesses of 200 nm, 250 nm, 300 nm, 350 nm, and 400 nm. Furthermore, at 2.85 THz, there are −20.9 dB, −22 dB, −23.2 dB, −23.3 dB, and −28.4 dB, respectively, at the thicknesses of 200 nm, 250 nm, 300 nm, 350 nm, and 400 nm. Fig. 2(b1) and (b2) give the 2D radiation patterns in the E-plane and H-plane, respectively at 1.65 THz. As indicated in Fig. 2(b), radiation pattern variation is minimal.

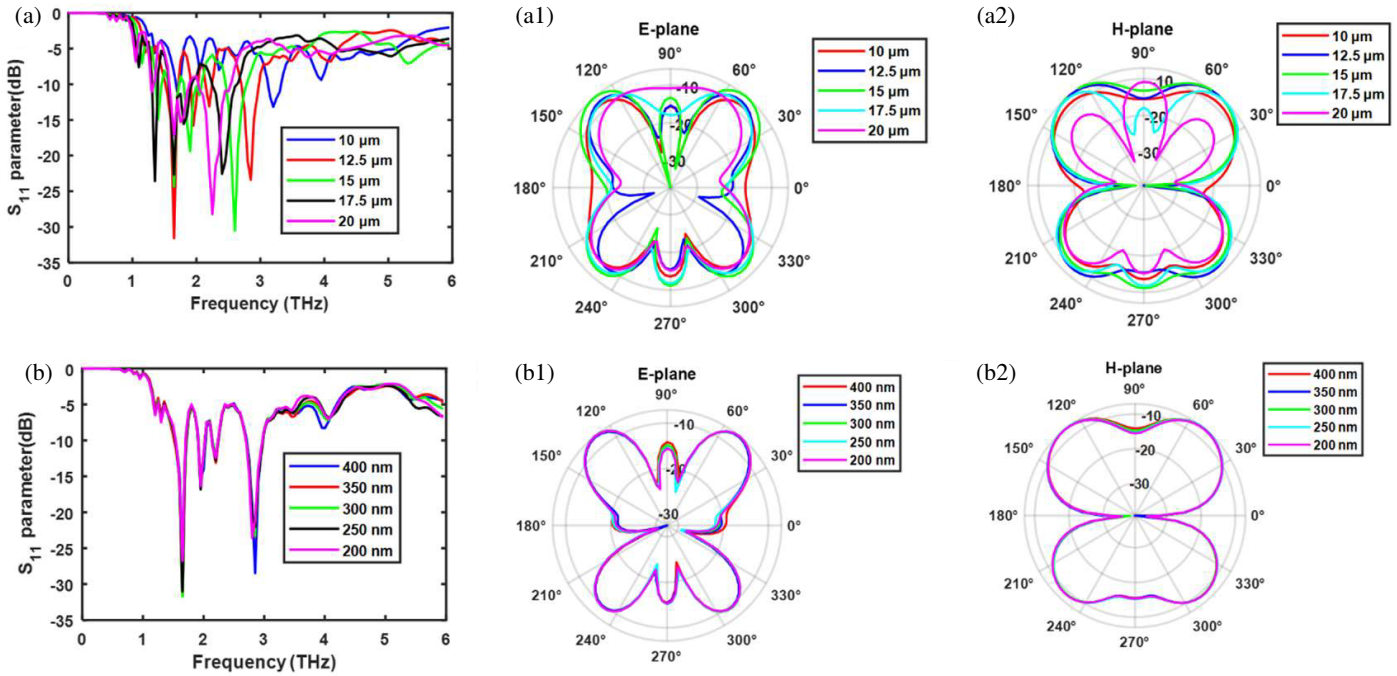

FIGURE 2. (a) S_{11} parameter of THz antenna with the variations in substrate thickness. (a1) E-plane variations in substrate thickness. (a2) H-plane variations in substrate thickness. (b) S_{11} parameter of THz antenna with the Au electrode thickness. (b1) E-plane variations in Au electrode thickness. (b2) H-plane variations in Au electrode thickness.

3.3. Antenna Length Study

Figure 3(a) depicts the S_{11} parameter of a THz antenna with variations in antenna length. The length of the antenna varies from 150 μm to 240 μm. In the antenna length study of the PCA, it is observed that as the length of the antenna decreases, the resonant frequency of the antenna increases. This leads to the change in the impedance of the antenna; hence, the reflection coefficient of the antenna varies. The feed line is matched to 50 Ω resistance. At the resonance, the impedance of the antenna is resistive, and it matches the feed impedance on the substrate. This effect decreases the reflections in the antenna. The results depict that for the antenna lengths 200 to 240 μm, the PCA resonates at 1.65 THz with −19.6 dB, −31.7 dB, −24.6 dB, and −16.1 dB, respectively, and at 150 μm, and it resonates at 1.7 THz with a −15.4 dB reflection coefficient. Further, at 2.85 THz, the proposed PCA resonates with a reflection coefficient of −23.5 dB, −23.2 dB, −18.8 dB, −32.6 dB, and −25.3 dB, respectively, for the antenna lengths 240 μm, 230 μm, 220 μm, 200 μm, and 150 μm. So, the study indicates that the optimal antenna length is 200 μm since at this frequency reflection is minimum. Figs. 3(a1) and (a2) give the 2D radiation patterns of the antenna length study in the E-plane and H-plane, respectively, with a resonant frequency of 2.85 THz.

3.4. Introducing Si Lens

Figure 3(b) depicts the S_{11} parameter of a THz antenna with a Si lens. The study indicates the effect of Si lenses on PCA. With this observation, the introduction of Si Lens gives more effectiveness to the PCA, and an increase in the transmittance of the antenna is also observed. The results depict that the introduction of the Si lens reduces the losses in the antenna even though it decreases the resonant frequency of the PCA. It is noticed that without the Si lens, PCA resonates at 1.35 THz with −24.2 dB, 1.65 THz with −22.1 dB, and 2.4 THz with −21.32 dB reflection coefficient. Additionally, with the Si lens having a radius of W, PCA resonates at 2.15 THz with a −30.2 dB reflection coefficient. Figs. 3(b1) and (b2) give a 2D radiation pattern in both the E-plane and H-plane with a frequency of 2.15 THz. It is observed that the radiation patterns of both the electric field and magnetic field plane change as the Si lens is introduced. Further, simulation is performed using various values of the radius of the lens, such as $W/2$, $W/3$, and $W/4$. The study reveals that at 2.15 THz with a radius of $W/3$, the proposed PCA exhibits a reflection coefficient of −30.2 dB, which is much improved compared to PCA without a lens.

3.5. Various Designs of PCA

The S_{11} parameters of different shapes of THz antennas are compared in Fig. 4(a). The structures discussed are H-shaped, bow-tie, and normal dipole structures. In this study, the bow-tie structure has more efficiency than other structures, which exhibit over −37 dB with a 2.05 THz resonant frequency. A comparison of H-shaped, bowtie, and dipole PCA designs is tabulated in Table 4. Figs. 4(a1) and (a2) give the 2D radiation patterns of various designs with an E-plane and H-plane at a frequency of 2.05 THz, which gives a similar change in radiation pattern compared to other factors.

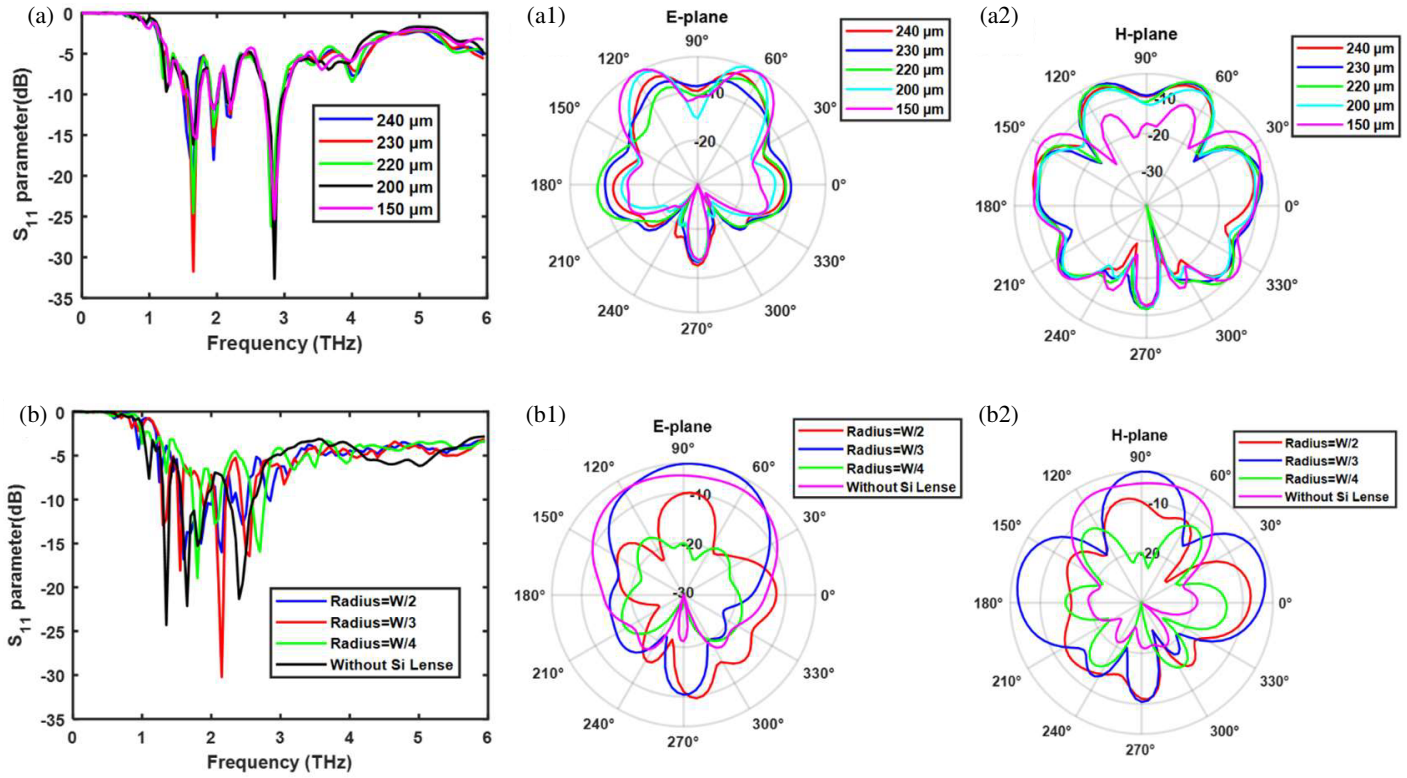

FIGURE 3. (a) S_{11} parameter of THz antenna with the variations in antenna length. (a1) E-plane variations in antenna length. (a2) H-plane variations in antenna length. (b) Comparison of S_{11} parameter of THz antenna without and with Si lens. (b1) Comparison of E-planes of THz antenna without and with Si lens. (b2) Comparison of H-planes of THz antenna without and with Si lens.

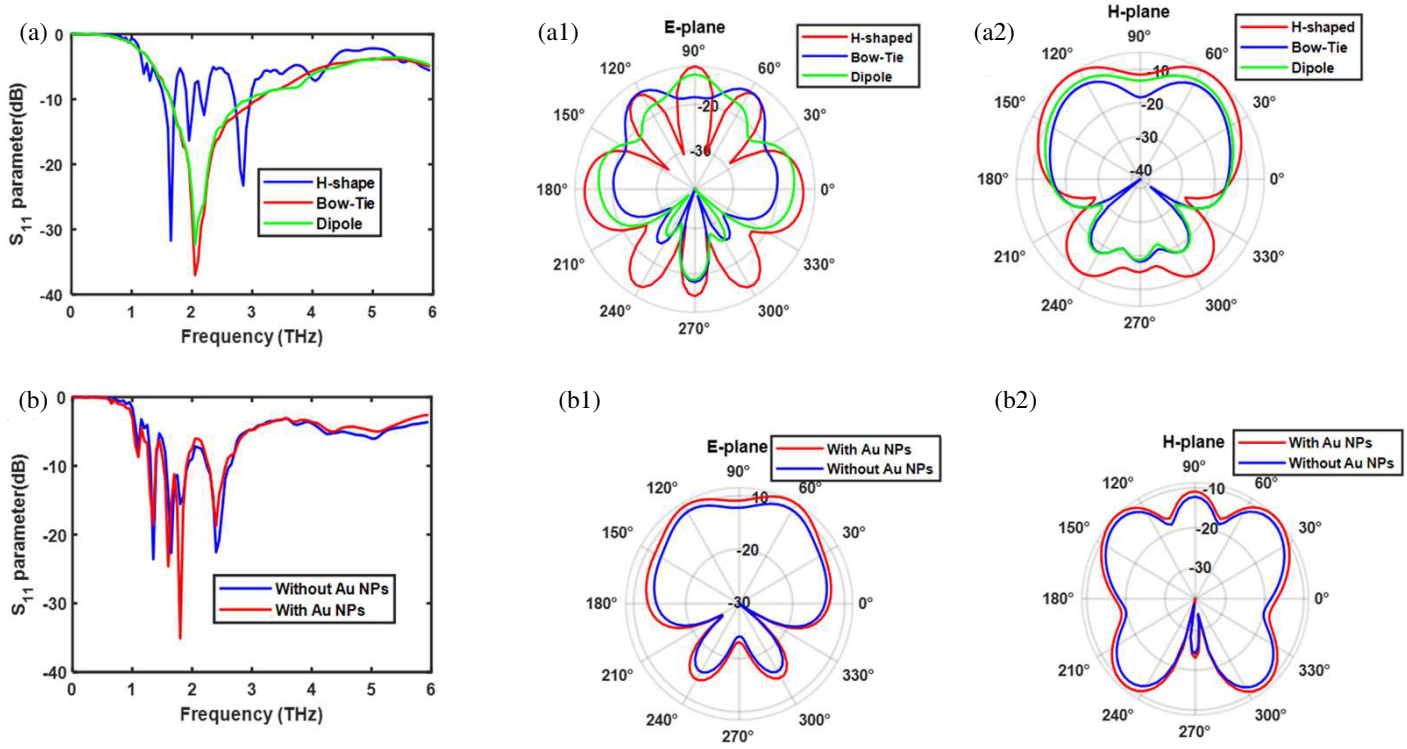

FIGURE 4. (a) S_{11} parameter of PCA with various designs of dipole structure. (a1) E-plane of PCA with various designs of dipole structure. (a2) H-planes of PCA with various designs of dipole structure. (b) Comparison of S_{11} parameter of THz antenna without and with nanopatterned PCA at substrate thickness 17.5 μm. (b1) Comparison of E-planes of nanopatterned PCA with substrate thickness 17.5 μm. (b2) Comparison of E-planes of nanopatterned PCA with substrate thickness 17.5 μm.

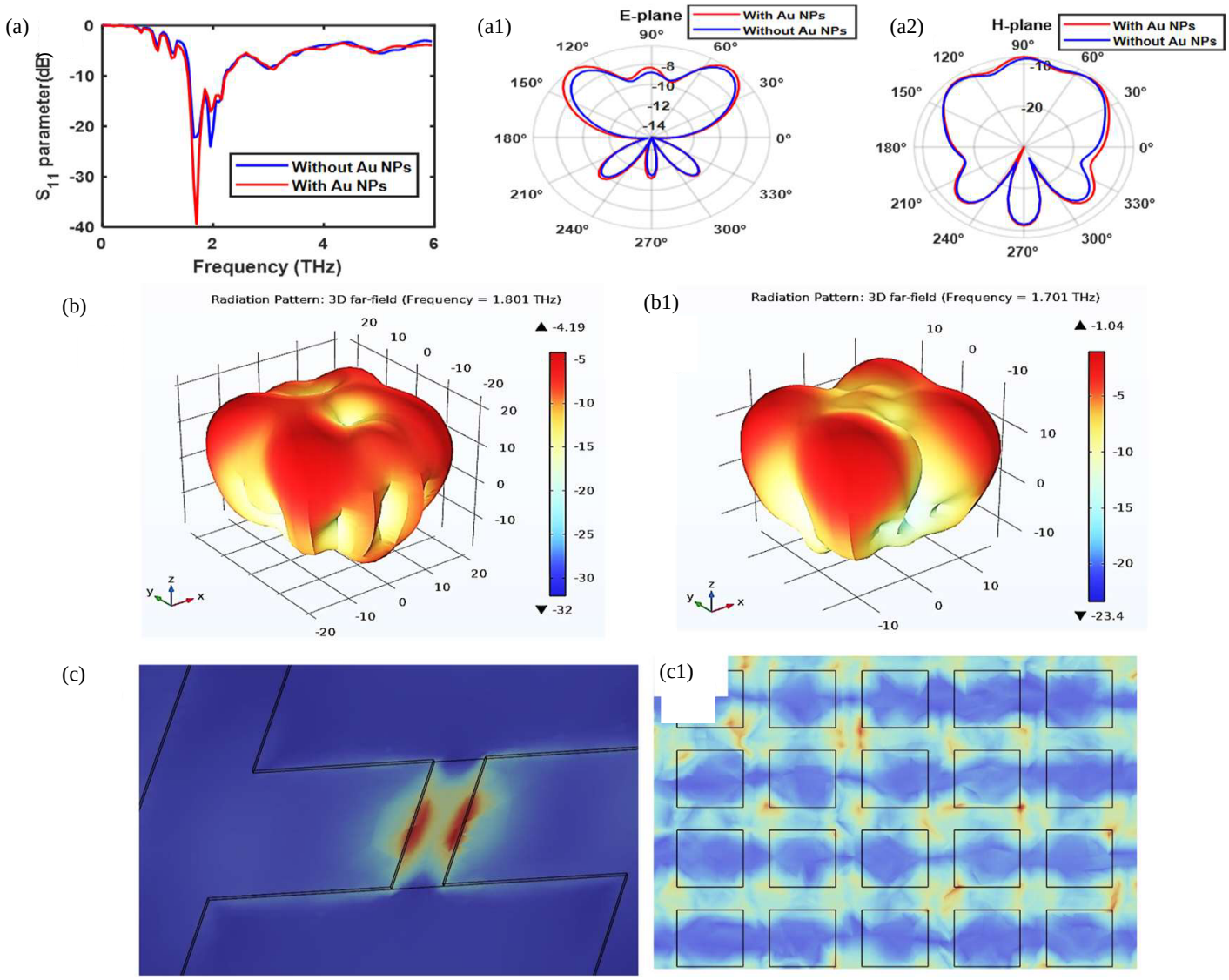

FIGURE 5. (a) Comparison of S_{11} parameter of THz antenna without and with nanopatterned PCA at substrate thickness 25 µm. (a1) Comparison of E-planes of nanopatterned PCA with substrate thickness 25 µm. (a2) Comparison of E-planes of nanopatterned PCA with substrate thickness 25 µm. (b) 3D Radiation pattern at substrate thickness 17.5 µm. (b1) 3D Radiation Pattern at substrate thickness 25 µm. (c) Surface current density of PCA gap without nanopattern. (c1) Surface current density of PCA gap with nanopattern.

TABLE 4. Comparison of various types of PCA.

Design	Frequency	Reflection Coefficient
H-shaped	1.65 THz	−31.75 dB
	2.8 THz	−20.86 dB
Bowtie	2.05 THz	−37.03 dB
Dipole	2.05 THz	−32.37 dB

3.6. Nanopatterned PCA

The H-shaped antenna is used for the analysis of nanopatterned PCA since it is a conventionally used structure in most of the systems, and it has a simple geometry compared to bow tie. The variation in thickness of the substrate study is conducted specifically for the nanopatterning PCA, and the results are depicted in Fig. 4(b) for the thickness of 17.5 µm. The various substrate thickness values considered are 2.5 µm, 10 µm, 17.5 µm, 25 µm, and 32.5 µm. Here, the thickness of the substrate study was conducted specifically for the nano-patterning. This allows us to analyze the data not only in the decoration but also in the effect of the thickness of the substrate with pattering. Also, the 2D radiation pattern of this study is given in Figs. 4(b1) and (b2) for E-plane and H-plane at 1.8 THz, respectively. This shows the drastic change in radiation with thickness. In this simulation, a nanopattern is decorated in the gap to increase efficiency. From the simulation, shown in Fig. 4(b), it is seen that there is a difference between the S_{11} parameter and the resonant frequency of 1.8 THz. The decoration of nano-patterns includes a size of 500 nm and a 40 nm thickness, and the distance between nanoparticles is over 200 nm. Here, the thickness of the substrate is 17.5 m. Figs. 4(b1) and (b2) give the 2D radiation pattern with and without nanopatterning; the E-plane and H-

TABLE 5. Comparison of the proposed PCA with the literature.

Reference	Material	Enhancement technique	Frequency (THz)	S_{11} (dB)	Efficiency
[22]	Gold, SI-GaAs	Bowtie	340	—	0.66
[23]	Gold, SI-GaAs	Manganese Ferrite Nanoparticles coating	0–5	—	—
[24]	Gold, Silicon nitride, LT-GaAs	ZnO Nanorods	0.1–1.2	−20.96	4-fold increase
[25]	Gold, LT-GaAs	Au nano-islands	0–4	—	40% improvement
[28]	Gold, InP	optical waveguides	0–5	—	22-fold increase
[51]	Silver, GaAs	Rectangular	2.067	−30	—
Proposed	Gold, LT-GaAs	Nanopattern	1.65 THz	−31.75	0.98

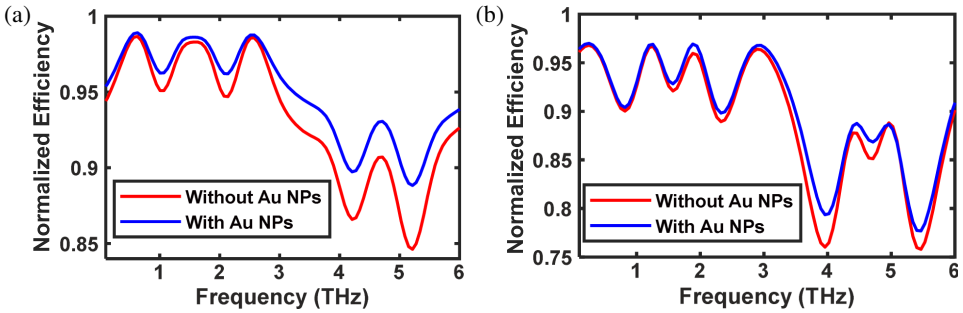

FIGURE 6. Normalized efficiency of the proposed photoconductive antenna at (a) 17.5 µm, (b) 25 µm.

plane are included with a resonant frequency of 1.8 THz. It shows that with a nanopattern, the radiation is reduced.

The above-mentioned process is repeated for 25 µm of thickness, and Fig. 5(a) depicts the reflection coefficient of the PCA. It is observed that as the size of the pattern is the same as above, to get enhanced efficiency, the distance between nanoparticles needs to be increased. Here, the distance between nanoparticles is over 800 nm with a 17 dB reduction in the reflection at the 1.7 THz resonant frequency. Figs. 5(a1) and (a2) give the 2D radiation patterns of the E-plane and H-plane, respectively. As the thickness of the substrate increased and the gap increased, the radiation pattern became similar in nature with a resonant frequency of 1.7 THz.

Figures 5(b) and (b1) show the 3D radiation patterns of different thicknesses of substrate, and the gap between the nanopatterns is changed for the purpose of increasing efficiency. It shows the difference in radiation pattern when thickness is increased. The advantage of increased thickness is that it shows a similar radiation pattern with and without nanopatterning. The introduction of the nanopattern increased the efficiency. Here, the nanostructure used is thin gold metal. So, these nanopatterns increase the surface plasmon of the PCA, which generates electron-hole pairs in the gap due to the nanopattern. In normal conditions, electron-hole pair generation and surface plasmon effect decrease as the gap increases, as shown in Fig. 5(c), which causes THz enhancement in the PCA. This is why, without a nanopattern, the THz enhancement is less. There are multiple options, such as structural parametric changes, changing the gap length of the dipole structure, the introduction of a semi-spherical Si lens, and various shapes of the dipole structure. However, these introductions have their limits, and due to these reasons, it is probable that they introduce a new idea that could change drastically in its effect.

With introducing the nanopattern, homogenous pattern formation is complex while looking into its practical purpose. It is observed that nanopatterning causes mutual edge coupling, as shown in Fig. 5(c1) of each nanopattern. As the distance increases between the patterns, these coupling effect reduction phenomena are also observed. From the first simulation with a substrate thickness of 17.5 m, it is seen that there is a difference of 11.6 dB in the S_{11} parameter at a resonant frequency of 1.8 THz with a 200 nm gap between the nanoparticles. A similar process is repeated for 25 m of the thickness of the substrate. It is observed that, as the size of the pattern is the same as above, to get enhanced efficiency, the distance between nanoparticles needs to be increased. Here, the distance between nanoparticles is over 800 nm. It is observed that there is a 17 dB reduction in the reflection at 1.7 THz resonant frequency. From this, it is observed that with an increase in the substrate thickness, the gap between the nanopatterns also increases. Fig. 6 shows the enhancement in the efficiency of the proposed photoconductive antenna at the substrate thicknesses 17.5 µm and 25 µm. Table 5 shows the comparison of the proposed antenna with the literature.

4. CONCLUSION

An H-shaped photoconductive antenna is designed and optimised using a COMSOL Multiphysics platform on an LT-GaAs substrate. The proposed antenna radiates at 1.35 THz with −24.2 dB, 1.65 THz with −22.1 dB, and 2.4 THz with −21.32 dB reflection coefficient. The results were obtained af-

ter the optimisation of the design parameters, such as the length and thickness of the antenna design materials. Further, to enhance the efficiency of the photoconductive antenna, a silicon lens is used in the gap between the electrodes to focus the light energy. In this technique, the minimum reflection coefficient of -30.2 dB is observed at 2.15 THz. Another technique of nanopatterning is used to increase the efficiency of the PCA. In this, gold nanoparticles are used to enhance the field concentration near the gap. The Au nanopatterned H-shaped PCA resonates at 1.7 THz with the reflection coefficient of -40 dB. The normalised efficiency of the photoconductive antenna using gold nanoparticles is observed as 0.98. The results indicate that the proposed H-shaped nanopatterned antenna can be used for terahertz applications.

REFERENCES

[1] Farhad, A. and J.-Y. Pyun, "Terahertz meets AI: The state of the art," *Sensors*, Vol. 23, No. 11, 5034, 2023.

[2] Jiang, W., Q. Zhou, J. He, M. A. Habibi, S. Melnyk, M. El-Absi, B. Han, M. D. Renzo, H. D. Schotten, F.-L. Luo, et al., "Terahertz communications and sensing for 6G and beyond: A comprehensive review," *IEEE Communications Surveys & Tutorials*, Vol. 26, No. 4, 2326–2381, 2024.

[3] Krozer, V., T. Löffler, J. Dall, A. Kusk, F. Eichhorn, R. K. Olsson, J. D. Buron, P. U. Jepsen, V. Zhurbenko, and T. Jensen, "Terahertz imaging systems with aperture synthesis techniques," *IEEE Transactions on Microwave Theory and Techniques*, Vol. 58, No. 7, 2027–2039, 2010.

[4] Armstrong, C. M., "The truth about terahertz," *IEEE Spectrum*, Vol. 49, No. 9, 36–41, 2012.

[5] Jha, K. R. and G. Singh, "Terahertz planar antennas for future wireless communication: A technical review," *Infrared Physics & Technology*, Vol. 60, 71–80, 2013.

[6] Liu, J., W.-H. Fan, X. Chen, and J. Xie, "Identification of high explosive RDX using terahertz imaging and spectral fingerprints," in *Journal of Physics: Conference Series*, Vol. 680, No. 1, 012030, 2016.

[7] Kurmi, Y. and V. Chaurasia, "Hidden explosive detection systems for vehicle," *International Journal of Computer Applications*, Vol. 130, No. 10, 16–19, 2015.

[8] Skvortsov, L. A., "Standoff detection of hidden explosives and cold and fire arms by terahertz time-domain spectroscopy and active spectral imaging," *Journal of Applied Spectroscopy*, Vol. 81, No. 5, 725–749, 2014.

[9] Piprek, J., *Semiconductor Optoelectronic Devices: Introduction to Physics and Simulation*, Academic Press, 2003.

[10] Tani, M., M. Herrmann, and K. Sakai, "Generation and detection of terahertzpulsed radiation with photoconductive antennas and its application toimaging," *Measurement Science and Technology*, Vol. 13, No. 11, 1739, 2002.

[11] Yu, C., S. Fan, Y. Sun, and E. Pickwell-MacPherson, "The potential of terahertz imaging for cancer diagnosis: A review of investigations to date," *Quantitative Imaging in Medicine and Surgery*, Vol. 2, No. 1, 33–45, 2012.

[12] Cai, Y., I. Brener, J. Lopata, J. Wynn, L. Pfeiffer, and J. Federici, "Design and performance of singular electric field terahertz photoconducting antennas," *Applied Physics Letters*, Vol. 71, No. 15, 2076–2078, 1997.

[13] Surdi, H., A. Singh, and S. S. Prabhu, "Enhancement of terahertz emission using AuGe nano-patterns," in *Proceedings of the 2013 COMSOL Conference in Bangalore*, 2013.

[14] Lewis, R., "Photoconductive antennas for terahertz applications," Safa O. Kasap (ed.), Vol. 1: Fundamentals, Wiley, 2022.

[15] Kumar, A., "A review of design and analysis for various shaped antenna in terahertz and subterahertz applications," *Turkish Journal of Computer and Mathematics Education*, Vol. 12, No. 8, 2053–2071, 2021.

[16] Russakoff, G., "A derivation of the macroscopic Maxwell equations," *American Journal of Physics*, Vol. 38, No. 10, 1188–1195, 1970.

[17] Maier, S. A., *Plasmonics: Fundamentals and Applications*, Springer, 2007.

[18] Indhu, A. R., L. Keerthana, and G. Dharmalingam, "Plasmonic nanotechnology for photothermal applications — An evaluation," *Beilstein Journal of Nanotechnology*, Vol. 14, No. 1, 380–419, 2023.

[19] Visser, H. J., *Antenna Theory and Applications*, John Wiley & Sons, 2012.

[20] Balanis, C. A., *Modern Antenna Handbook*, John Wiley & Sons, 2011.

[21] Smith, P. R., D. H. Auston, and M. C. Nuss, "Subpicosecond photoconducting dipole antennas," *IEEE Journal of Quantum Electronics*, Vol. 24, No. 2, 255–260, Feb. 1988.

[22] Park, S., K. Jin, J. Ye, and K. H. Jeong, "Nanoplasmonic photoconductive antenna for high power terahertz emission," in *2011 16th International Solid-State Sensors, Actuators and Microsystems Conference*, 2498–2501, Beijing, China, 2011.

[23] Lai, W., O. M. Abdulmunem, P. D. Pino, B. Pelaz, W. J. Parak, Q. Zhang, and H. Zhang, "Enhanced terahertz radiation generation of photoconductive antennas based on manganese ferrite nanoparticles," *Scientific Reports*, Vol. 7, No. 1, 46261, 2017.

[24] Bashirpour, M., M. Forouzmehr, S. E. Hosseininejad, M. Kolahdouz, and M. Neshat, "Improvement of terahertz photoconductive antenna using optical antenna array of ZnO nanorods," *Scientific Reports*, Vol. 9, No. 1, 1414, 2019.

[25] Murakami, H., T. Takarada, and M. Tonouchi, "Low-temperature GaAs-based plasmonic photoconductive terahertz detector with Au nano-islands," *Photonics Research*, Vol. 8, No. 9, 1448–1456, 2020.

[26] Arora, N., A. Bandyopadhyay, and A. Sengupta, "Modeling and optimization of THz photoconductive antenna," in *COMSOL Multiphysics Conference*, Bangalore, 2018.

[27] De Vetter, A., C. Song, M. Mičica, J. Tignon, J. Mangeney, J. Palomo, and S. Dhillon, "Large area terahertz digitated photoconductive antennas based on a single high resistivity metal and nanoplasmonic electrode," *Photonics and Nanostructures — Fundamentals and Applications*, Vol. 59, 101248, 2024.

[28] Deumer, M., S. Nellen, S. Berrios, S. Breuer, S. Keyvaninia, L. Liebermeister, M. Schell, and R. B. Kohlhaas, "Advancing terahertz photomixers through the integration of photoconductive antennas with optical waveguides," *APL Photonics*, Vol. 10, No. 3, 036105, 2025.

[29] Chen, Y., F. Qin, L. Liu, Z. Zhao, P. Li, Y. Sun, W. Liu, and Y. Wang, "0.4 THz broadband terahertz noise source based on photoconductive antennas," *Photonics*, Vol. 12, No. 3, 252, 2025.

[30] Bashirpour, M., S. Ghorbani, M. Kolahdouz, M. Neshat, M. Masnadi-Shirazi, and H. Aghababa, "Significant performance improvement of a terahertz photoconductive antenna using a hybrid structure," *RSC Advances*, Vol. 7, No. 83, 53 010–53 017, 2017.

[31] Malhotra, I., K. R. Jha, and G. Singh, "Analysis of highly directive photoconductive dipole antenna at terahertz frequency for sensing and imaging applications," *Optics Communications*, Vol.

397, 129–139, 2017.

[32] Martin, M. and E. R. Brown, "Critical comparison of GaAs and InGaAs THz photoconductors," in *Proceedings of SPIE*, Vol. 8261, 826102, 2012.

[33] Kostakis, I., D. Saeedkia, and M. Missous, "Characterization of low temperature InGaAs-InAlAs semiconductor photo mixers at 1.55 μm wavelength illumination for terahertz generation and detection," *Journal of Applied Physics*, Vol. 111, No. 10, 103105, 2012.

[34] Baker, C., I. S. Gregory, W. R. Tribe, I. V. Bradley, M. J. Evans, E. H. Linfield, and M. Missous, "Highly resistive annealed low-temperature-grown InGaAs with sub-500 fs carrier lifetimes," *Applied Physics Letters*, Vol. 85, No. 21, 4965–4967, 2004.

[35] Auston, D. H., K. P. Cheung, and P. R. Smith, "Picosecond photoconducting Hertzian dipoles," *Applied Physics Letters*, Vol. 45, No. 3, 284–286, 1984.

[36] Sze, S. M. and K. K. Ng, *Physics of Semiconductor Devices*, Wiley-Interscience, 2007.

[37] Taylor, Z. D., E. R. Brown, J. E. Bjarnason, M. P. Hanson, and A. C. Gossard, "Resonant-optical-cavity photoconductive switch with 0.5% conversion efficiency and 1.0 w peak power," *Optics Letters*, Vol. 31, No. 11, 1729–1731, 2006.

[38] Gupta, S., J. F. Whitaker, and G. A. Mourou, "Ultrafast carrier dynamics in III-V semiconductors grown by molecular-beam epitaxy at very low substrate temperatures," *IEEE Journal of Quantum Electronics*, Vol. 28, No. 10, 2464–2472, 1992.

[39] Gupta, S., M. Y. Frankel, J. A. Valdmanis, J. F. Whitaker, G. A. Mourou, F. W. Smith, and A. R. Calawa, "Subpicosecond carrier lifetime in GaAs grown by molecular beam epitaxy at low temperatures," *Applied Physics Letters*, Vol. 59, No. 25, 3276–3278, 1991.

[40] Khiabani, N., "Modelling, design and characterisation of terahertz photoconductive antennas," The University of Liverpool, United Kingdom , 2013.

[41] Tani, M., S. Matsuura, K. Sakai, and S.-i. Nakashima, "Emission characteristics of photoconductive antennas based on low-temperature-grown GaAs and semi-insulating GaAs," *Applied Optics*, Vol. 36, No. 30, 7853–7859, 1997.

[42] Stone, M. R., M. Naftaly, R. E. Miles, J. R. Fletcher, and D. P. Steenson, "Electrical and radiation characteristics of semilarge photoconductive terahertz emitters," *IEEE Transactions on Microwave Theory and Techniques*, Vol. 52, No. 10, 2420–2429, 2004.

[43] Stibal, R., J. Windscheif, and W. Jantz, "Contactless evaluation of semi-insulating GaAs wafer resistivity using the time-dependent charge measurement," *Semiconductor Science and Technology*, Vol. 6, No. 10, 995, 1991.

[44] Beard, M. C., G. M. Turner, and C. A. Schmuttenmaer, "Subpicosecond carrier dynamics in low-temperature grown GaAs as measured by time-resolved terahertz spectroscopy," *Journal of Applied Physics*, Vol. 90, No. 12, 5915–5923, 2001.

[45] Smith, F. W., H. Q. Le, V. Diadiuk, M. A. Hollis, A. R. Calawa, S. Gupta, M. Frankel, D. R. Dykaar, G. A. Mourou, and T. Y. Hsiang, "Picosecond GaAs-based photoconductive optoelectronic detectors," *Applied Physics Letters*, Vol. 54, No. 10, 890–892, 1989.

[46] Jo, S. J., S.-G. Ihn, J.-I. Song, K.-J. Yee, and D.-H. Lee, "Carrier dynamics of low-temperature-grown $In_{0.53}Ga_{0.47}As$ on GaAs using an InGaAlAs metamorphic buffer," *Applied Physics Letters*, Vol. 86, No. 11, 111903, 2005.

[47] Takazato, A., M. Kamakura, T. Matsui, J. Kitagawa, and Y. Kadoya, "Terahertz wave emission and detection using photoconductive antennas made on low-temperature-grown InGaAs with 1.56 μm pulse excitation," *Applied Physics Letters*, Vol. 91, No. 1, 011102, 2007.

[48] Johnson, P. B. and R.-W. Christy, "Optical constants of the noble metals," *Physical Review B*, Vol. 6, No. 12, 4370, 1972.

[49] Green, M. A. and M. J. Keevers, "Optical properties of intrinsic silicon at 300 K," *Progress in Photovoltaics: Research and Applications*, Vol. 3, No. 3, 189–192, 1995.

[50] Rosenblatt, G., B. Simkhovich, G. Bartal, and M. Orenstein, "Nonmodal plasmonics: Controlling the forced optical response of nanostructures," *Physical Review X*, Vol. 10, No. 1, 011071, 2020.

[51] Pratheep, R., S. S. Harish, V. Rathinasamy, et al., "Terahertz photoconductive antenna for sensing and imaging applications," *2024 International Conference on Wireless Communications Signal Processing and Networking (WiSPNET)*, 1–4, Chennai, India, 2024.